A Direct Wave-Drive Thruster using the Magnetosonic Mode

IEPC-2015-115/ISTS-2015-b-115

Presented at Joint Conference of 30th International Symposium on Space Technology and Science, 34th International Electric Propulsion Conference and 6th Nano-satellite Symposium
Hyogo-Kobe, Japan
July 4–10, 2015

Matthew S. Feldman* and Benjamin A. Jorns † and Edgar Y. Choueiri‡
Electric Propulsion and Plasma Dynamics Lab, Princeton, NJ, 08544, USA
Jet Propulsion Laboratory, California Institute of Technology, Pasadena, CA 91109, USA

The generalized relations for the scaling of thrust and efficiency are derived for a Direct Wave-Drive Thruster (DWDT), and the magnetosonic wave is proposed as an ideal candidate for driving a DWDT. The magnetosonic wave is shown to be capable of carrying substantial momentum while remaining linear, which prevents potential coupling losses from the wave-launching antenna. The thrust coefficient for a magnetosonic mode driven DWDT is then calculated, which shows that optimal antenna-plasma coupling occurs when the characteristic wavelength of the magnetosonic wave is smaller than the length scale of the thruster. The propagation of the magnetosonic wave in the exhaust plume is analyzed with ray optics to determine the overall plasma structure in a wave-dominated thruster. By including mass continuity, the plasma is found to maintain a constant impedance as the background magnetic field decays. This process allows the wave to propagate without reflection until it can be absorbed at the lower hybrid resonance. An anisotropic Péclet number comparing wave-driven mass advection to cross-field diffusion wall losses is then derived, which shows that a wave-dominated accelerator can be achieved for low power levels.

*Ph.D. Candidate, Princeton University, Department of Mechanical and Aerospace Engineering, feldmanm@princeton.edu.
†Associate Engineer, Electric Propulsion Group, Jet Propulsion Laboratory, benjamin.a.jorns@jpl.nasa.gov
‡Professor, Princeton University, Department of Mechanical and Aerospace Engineering, Chief Scientist EPPDyL, choueiri@princeton.edu

Nomenclature

$\overline{\overline{P}}_{EM_{ij}}$	= maxwell stress tensor
T	= thrust
P	= power
η	= efficiency
E, B, A	= electric, magnetic, vector potential field
J_a	= wave-launching antenna current
C_T, R_{eff}	= thrust and resistive loss coefficients
$\dot{m}$	= total mass flow rate
ω, k	= wave frequency and wavenumber
$\tilde{\rho}, \tilde{v}, \tilde{B}$	= oscillation amplitudes of density, velocity, and magnetic field
c, μ_0	= speed of light and permeability of free space
$\rho, \mathcal{P}, \mathcal{E}$	= mass, momentum, and energy density
$\dot{\mathcal{M}}, \dot{\mathcal{P}}, \dot{\mathcal{E}}$	= mass, momentum, and energy fluxes
p	= pressure
x, y, z	= coordinates
L, W, H	= thruster length, width, height in the x, y, z coordinates
σ, ϵ	= conductivity and dielectric constant
ν_e	= Electron collision frequency
γ	= antenna-plasma coupling parameter
Pec	= Péclet number
$D_\perp$	= cross-field diffusion coefficient

I. Introduction

The Direct Wave-Drive Thruster (DWDT) is a new propulsion concept that utilizes waves for direct momentum transfer to a plasma.[1,2] Like other waves-based and inductive accelerators,[3–7] it is electrodeless, and therefore can avoid potentially life-limiting erosion processes. Previous waves-based thruster concepts have used various waves to heat a plasma and obtain thrust via expansion through a magnetic nozzle.[3–5] In contrast, a DWDT attempts to avoid limitations associated with magnetic nozzles by coupling wave momentum directly into a plasma for acceleration. In general, this momentum coupling can be done via an inductive antenna, which is qualitatively similar to antennas used in Pulsed Inductive Thrusters (PIT).[6,7] However, instead of discharging in a single pulse, the wave-launching antenna operates continuously to inject momentum directly into the plasma.

Previous work has examined the potential for RF energy to directly accelerate or confine a plasma,[2,8,9] but until recently, little effort has gone in to the development of a feasible thruster concept. Most recently, we examined a DWDT in its simplest form in terms of the antenna-plasma interaction for the reflected ordinary wave and found that efficiencies of 50% were theoretically possible at moderate power levels of 5 kW.[1] However, that simplified analysis ignored any effects from a confining magnetic field, as well as any relevant propagating wave dynamics.

Some work on DWDTs has focused on propagating electrostatic waves in the context of the ponderomotive thruster.[2] However, this work did not include the effects of mass continuity in the plasma exhaust plume or any antenna-plasma interactions. Additionally, the most effective wave modes for acceleration have not been identified.

In order to present a comprehensive picture of a DWDT in preparation for a proof-of-concept experiment, we will layout the generalized scaling relations for thrust and efficiency and motivate the use of the magnetosonic mode as an ideal wave mode for driving this accelerator. We then identify key parameters that govern the performance of the magnetosonic mode driven DWDT, including the scaling of the thrust coefficient and the critical power at which wave-driven mass advection dominates wall losses. Finally, we describe the plasma dynamics in the exhaust plume and demonstrate that the wave momentum is not reflected.

The layout for this paper will proceed as follows. In Section II, we describe the DWDT concept and generalized scaling laws. In Section III, we motivate the magnetosonic wave as particularly suited for plasma acceleration. In Section IV, we layout an idealized geometry for launching the magnetosonic wave and calculate the scaling of the thrust coefficients in the limits of large and small wavelengths. In Section V, we describe the wave behavior in the exhaust plume and the eventual wave absorption mechanism. In Section VI, we calculate an anisotropic Péclet number relating the wave-driven mass advection to diffusive wall losses. In Section VII, we summarize the design considerations stemming for this analysis for a future proof-of-concept experiment.

II. DWDT Scaling Behavior

In its simplest form, the DWDT consists of a confining background magnetic field and a wave-launching antenna. A simple 1D channel is shown in Figure 1. The background B-field confines plasma away from the walls and also can be tuned to create modes of interest inside of the thruster that can be coupled to by the wave-launching antenna. This antenna is responsible for all momentum transferred to the plasma and acquired by the exhaust. We previously modeled the antenna-plasma interaction for a specific annular geometry and the non-propagating ordinary mode.[1] However, the general scaling relations can be described for arbitrary configurations.

We can calculate the total thrust by time-averaging the electromagnetic pressure exerted on the plasma, i.e.:

$$T = \int_S \langle \overline{\overline{P}}_{EM_{ij}} \rangle \cdot dA, \tag{1}$$

where $\overline{\overline{P}}_{EM_{ij}}$ is the maxwell stress tensor:

$$\overline{\overline{P}}_{EM_{ij}} = \epsilon_0 (E_i E_j - \frac{1}{2}\delta_{ij} E^2) + \frac{1}{\mu_0}(B_i B_j - \frac{1}{2}\delta_{ij} B^2). \tag{2}$$

In general, the electromagnetic pressure is dependent on the geometry of the system, excitation frequency, and the plasma response. However, in a linear response, the magnitudes of the oscillating electric and

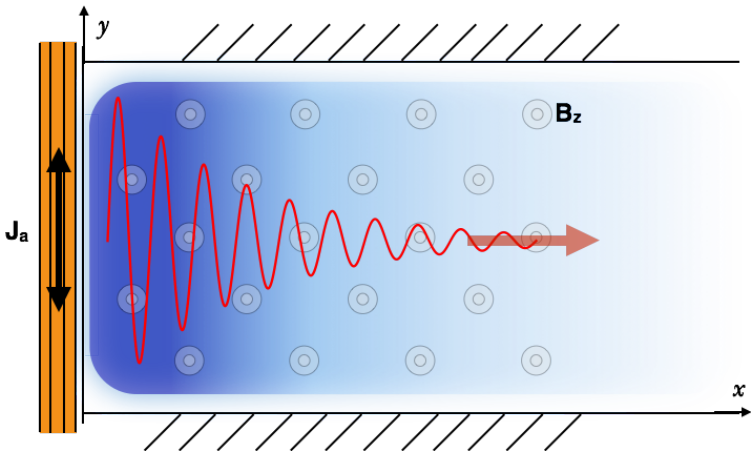

Figure 1. The Direct Wave-Drive Thruster. Plasma is confined in a thruster channel by way of a background magnetic field in the $\hat{z}$-direction. A wave-launching antenna structure is placed behind the channel, which generates a propagating mode in the positive $\hat{x}$-direction. In steady state, the propagating mode accelerates the plasma across field lines and out of the thruster.

magnetic fields are proportional to the magnitude of the exciting current in the wave-launching antenna, J_a. Therefore, the total pressure, and also total thrust, must be proportional to current squared:

$$T = C_T J_a^2, \tag{3}$$

where C_T is a thrust coefficient that includes the effects of geometry and plasma response.

We calculate the scaling of thrust efficiency by determining the total thrust power and the dissipation due to various loss mechanisms. Thrust power is given by

$$P_T = \frac{T^2}{2\dot{m}}. \tag{4}$$

The dominant loss mechanisms are resistive and radiative, which scale as

$$P_L = R_{\text{eff}} J_a^2. \tag{5}$$

Therefore, efficiency can be modeled as

$$\eta = \frac{P_T}{P_T + P_L} = \frac{1}{1 + \frac{2\dot{m}R_{\text{eff}}}{C_T^2 J_a^2}}, \tag{6}$$

where $\dot{m}$ is the mass flow, and R_{eff} is the effective total resistance associated with heating and radiative loss mechanisms, which like C_T can have a complicated dependence on the geometry and plasma dynamics.

III. The Magnetosonic Wave

Previous work has suggested driving DWDTs with electrostatic modes.[1,2] These waves have a high ratio of momentum to energy density and therefore are capable of driving high thrust-to-power accelerators. This is also the case for the compressional Alfvén (or magnetosonic) wave. However, unlike electrostatic modes, the magnetosonic wave can transmit significant momentum while remaining linear.

A. Thrust-to-Power Ratio

The most promising waves of interest for DWDTs are those capable of producing exhaust velocities useful for propulsive applications, typically between 10-100 km/s for electric accelerators. Since the momentum and energy in the exhaust come entirely from the driving wave, the thrust-to-power ratio for a DWDT is controlled by the wave momentum and energy, given by:

$$P = \hbar k, \tag{7}$$

$$E = \hbar\omega. \tag{8}$$

Therefore, the equivalent thrust-to-power ratio for a propagating mode is

$$\frac{T}{P} = \frac{k}{\omega} = \frac{1}{v_p}. \tag{9}$$

Since T/P also scales as $1/v_{\text{ex}}$, the final exhaust velocity of the plume will be proportional to the phase velocity of our targeted wave mode. In general, wave modes with appropriate phase velocities are those targeting acoustic ion motion.

B. Momentum Density in Ion Acoustic and Magnetosonic Waves

Electrostatic and magnetosonic modes can both reach phase velocities of interest. However, while electrostatic waves carry momentum via a thermal restoring force, magnetosonic waves rely on the background magnetic field to propagate. The reliance on thermal energy for wave propagation limits the achievable thrust for electrostatic waves. This is readily seen by comparing the momentum flux of the electrostatic ion cyclotron and magnetosonic waves to the background plasma pressure.

The momentum flux of a given wave is a product of the group velocity and the momentum density. Since the momentum is primarily contained in the oscillating particles,[10] the momentum density is

$$\mathcal{P} = \langle \rho v \rangle = \langle \tilde{\rho}\tilde{v} \rangle. \tag{10}$$

From the linearized continuity equation,

$$-i\omega\tilde{\rho} + ik\bar{\rho}\tilde{v} = 0, \tag{11}$$

we can time average and rewrite Equation 10 as

$$\mathcal{P} = \frac{1}{2}\frac{\tilde{\rho}^2}{\bar{\rho}}\frac{\omega}{k}. \tag{12}$$

The phase and group velocities of the electrostatic ion cyclotron and magnetosonic waves can be calculated from their respective dispersion relations

$$\omega^2 = \Omega_i^2 + v_s^2 k^2, \tag{13}$$

$$\omega^2 = v_A^2 k^2 = \frac{\bar{B}^2}{\mu_0 \bar{\rho}} k^2. \tag{14}$$

Therefore the momentum flux, $\dot{\mathcal{P}} = v_g \mathcal{P}$, for each wave is

$$\dot{\mathcal{P}}_{\text{EIC}} = \frac{1}{2}\frac{\tilde{\rho}^2}{\bar{\rho}} v_s^2, \tag{15}$$

$$\dot{\mathcal{P}}_{\text{MS}} = \frac{1}{2}\frac{\tilde{\rho}^2}{\bar{\rho}} v_A^2, \tag{16}$$

which can be simplified to

$$\dot{\mathcal{P}}_{\text{EIC}} = \frac{1}{2} p_{\text{th}} \frac{\tilde{\rho}^2}{\bar{\rho}^2}, \tag{17}$$

$$\dot{\mathcal{P}}_{\text{MS}} = \frac{1}{2} p_{\text{B}} \frac{\tilde{\rho}^2}{\bar{\rho}^2}. \tag{18}$$

For linear modes, $\tilde{\rho}/\bar{\rho} \ll 1$. As a result, the momentum flux of the linear electrostatic ion cyclotron wave is necessarily smaller than the thermal pressure already present in the plasma. In order to reach a regime where the wave propagation dominates the momentum transfer, the wave must be highly non-linear, and the density rarefactions will be large compared to the background density. This average lower density will tend to result in worse coupling between the wave-launching antenna and the plasma.[1]

However, the magnetosonic wave does not rely on thermal energy to propagate. With sufficiently large applied magnetic fields, this mode can carry significant momentum flux while remaining linear. Moreover, since we have direct control over the background magnetic strength and topology, we can tune the wave parameters as desired. This makes the magnetosonic wave ideal for driving a confined Direct Wave-Drive Thruster.

IV. Thrust Coefficient Scaling for the Magnetosonic DWDT

Previous work on the DWDT calculated C_T and R_{eff} for the evanescing ordinary mode and included a complicated annular geometry and resistive losses in the plasma itself.[1] We will proceed along the same path to determine the thrust coefficient for a magnetosonic mode driven DWDT in a simplified linear geometry, which will elucidate important nondimensional parameters that govern the antenna-plasma coupling.

The idealized geometry, shown in Figure 2, is uniform and infinite in the $\hat{y}$-direction. A constant background magnetic field is applied in the $\hat{z}$-direction with magnitude B_0. The wave-launching antenna is located at the $x = 0$ plane with a width of $2H$ and current in the $\hat{y}$-direction, oscillating with frequency ω and magnitude J_a. A semi-infinite slab of plasma is located at $x > l$ with density n_0 and an ion mass M. Additionally, we relax some of the constraints from our previous analysis[1] to allow electromagnetic modes to propagate both inside and outside the plasma. In this configuration, compressional Alfvén waves will be launched in the positive-$\hat{x}$ direction.

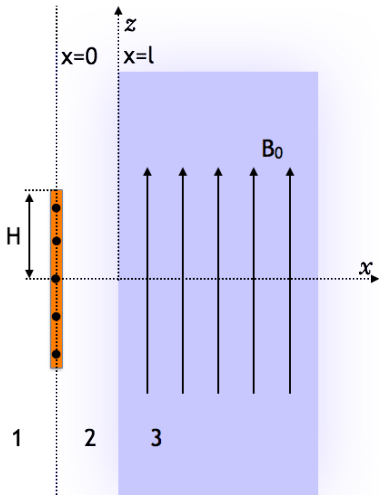

Figure 2. Simplified magnetosonic mode driven DWDT geometry. A semi-infinite plasma slab is placed at $x > l$ in a constant background magnetic field, $B_0\hat{z}$. A wave-launching antenna is located at $x = 0$ with a height, $2H$, in the $\hat{z}$-direction, and a total current in the $\hat{y}$-direction oscillating with frequency, ω, and magnitude, J_a. The geometry is assumed to be uniform and infinite in the $\hat{y}$-direction.

To determine the total force, we simply calculate the total electromagnetic fields and integrate the electromagnetic pressure over the surface of the plasma slab. These fields are most easily calculated via the wave equation for the magnetic vector potential,

$$\nabla^2 \mathbf{A} = \frac{1}{c^2}\frac{\partial^2}{\partial t^2}\mathbf{A} + \mu_0 \sigma_\omega \cdot \frac{\partial}{\partial t}\mathbf{A}, \tag{19}$$

where σ_ω is the complex, frequency-dependent conductivity of the plasma. In our simplified geometry, $\mathbf{A}$ has components in only the $\hat{y}$-direction, and we can further reduce the equation with a Fourier transform in the time domain by assuming $\mathbf{A} = A_y e^{-i\omega t}$, such that

$$\nabla^2 A_y + \frac{\omega^2}{c^2}\epsilon_\perp A_y = 0, \tag{20}$$

where $\epsilon_\perp$ is the cross field dielectric. In vacuum, $\epsilon_\perp$ is unity, and inside the plasma, $\epsilon_\perp = 1 + \frac{c^2}{v_A^2}$.[11] Before solving, we will follow previous convention[1] and nondimensionalize the domain by the antenna length scale, H, and the excitation frequency, ω, such that

$$\bar{x} = \tfrac{x}{H} \qquad \bar{z} = \tfrac{z}{H} \qquad \bar{l} = \tfrac{l}{H} \qquad \bar{k}_v = \tfrac{\omega H}{c} \qquad \bar{k}_a = \tfrac{\omega H}{v_A} \qquad \bar{A} = \tfrac{A}{\mu_0 J_a} \qquad \tau = \omega t \qquad \bar{\nabla} = H\nabla,$$

and Equation 20 becomes

$$\bar{\nabla}^2 \bar{A}_y + \bar{K}^2 \bar{A}_y = 0, \tag{21}$$

where

$$\bar{K}^2 = \begin{cases} \bar{k}_v^2 & \bar{x} < \bar{l} \\ \bar{k}_v^2 + \bar{k}_a^2 & \bar{x} > \bar{l} \end{cases}. \tag{22}$$

The full derivation for the spatial solution in the $\hat{\bar{x}} - \hat{\bar{z}}$ plane is in Appendix A and follows closely techniques used in previous works.[1,12,13] The result is a piecewise solution across the three regions behind the antenna, between the antenna and plasma, and in the plasma itself:

$$\bar{A}_{y1}(\bar{x}, \bar{z}, \bar{k}_v, \bar{k}_a, \bar{l}) = \int_0^\infty C_1 e^{-i\bar{k}_1\bar{x}} \cos(a\bar{z}) da, \tag{23}$$

$$\bar{A}_{y2}(\bar{x}, \bar{z}, \bar{k}_v, \bar{k}_a, \bar{l}) = \int_0^\infty (C_2 e^{i\bar{k}_1\bar{x}} + C_3 e^{-i\bar{k}_1\bar{x}}) \cos(a\bar{z}) da, \tag{24}$$

$$\bar{A}_{y3}(\bar{x}, \bar{z}, \bar{k}_v, \bar{k}_a, \bar{l}) = \int_0^\infty C_4 e^{i\bar{k}_2\bar{x}} \cos(a\bar{z}) da, \tag{25}$$

where

$$\bar{k}_1 = \sqrt{\bar{k}_v^2 - a^2}, \tag{26}$$

$$\bar{k}_2 = \sqrt{\bar{k}_v^2 + \bar{k}_a^2 - a^2}, \tag{27}$$

and a is the spatial separation constant. The coefficients, C_i, are derived in Appendix A:

$$C_1 = \frac{1}{i\pi} \frac{\sin a}{a} \frac{1}{\bar{k}_1} \left(1 + \frac{\bar{k}_1 - \bar{k}_2}{\bar{k}_1 + \bar{k}_2} e^{2i\bar{k}_1\bar{l}}\right), \tag{28}$$

$$C_2 = \frac{1}{i\pi} \frac{\sin a}{a} \frac{1}{\bar{k}_1} \tag{29}$$

$$C_3 = \frac{1}{i\pi} \frac{\sin a}{a} \frac{e^{2i\bar{k}_1\bar{l}}}{\bar{k}_1} \frac{\bar{k}_1 - \bar{k}_2}{\bar{k}_1 + \bar{k}_2}, \tag{30}$$

$$C_4 = \frac{2}{i\pi} \frac{\sin a}{a} \frac{e^{i(\bar{k}_1 - \bar{k}_2)\bar{l}}}{\bar{k}_1 + \bar{k}_2}. \tag{31}$$

The magnitude of $\bar{A}_y$ represents the size of the propagating wave mode, and thus the total electromagnetic pressure, which can be integrated at the plasma surface and time-averaged to determine a total thrust:

$$T = \frac{1}{8}\mu_0 J_a^2 \iint \bar{k}_a^2 \frac{1}{2} \|\bar{A}_y(\bar{x} = \bar{l})\|^2 d\bar{y} d\bar{z}. \tag{32}$$

Combining Equations 25, 27, 31, and 32, the total force on the plasma is

$$T = \frac{1}{8}\mu_0 J_a^2 \iint \frac{1}{2} \left\| \int_0^\infty \frac{2}{\pi} \frac{\sin a}{a} \frac{\bar{k}_a}{\bar{k}_1 + \bar{k}_2} e^{i\bar{k}_1\bar{l}} \cos(a\bar{z}) da \right\|^2 d\bar{y} d\bar{z}. \tag{33}$$

We now take the thruster to have finite width, W, such that the total thrust becomes

$$T = C_T J_a^2, \tag{34}$$

where

$$C_T = \frac{1}{8}\mu_0 \overline{W} \cdot \gamma(\bar{k}_a, \bar{k}_v, \bar{l}), \tag{35}$$

$\overline{W} = W/H$, and γ is a coupling coefficient between 0 and 1 given by

$$\gamma(\bar{k}_a, \bar{k}_v, \bar{l}) = \frac{1}{2} \int_{-\infty}^\infty \left\| \int_0^\infty \frac{2}{\pi} \frac{\sin a}{a} \frac{\bar{k}_a}{\bar{k}_1 + \bar{k}_2} e^{i\bar{k}_1\bar{l}} \cos(a\bar{z}) da \right\|^2 d\bar{z}. \tag{36}$$

We proceed with a parameter space investigation of γ by varying the relevant non-dimensional quantities, $\bar{k}_a$, $\bar{k}_v$, and $\bar{l}$, and numerically integrating Equation 36. The normalized vacuum wavenumber, $\bar{k}_v$, is relatively small in any configuration and only varies with the overall size of the system. Additionally, our previous work has shown that the normalized stand-off length for the antenna, $\bar{l}$, should remain small for good coupling.[1] The normalized Alfvén wavenumber, $\bar{k}_a$, however, has not yet been investigated and is therefore the primary quantity of interest.

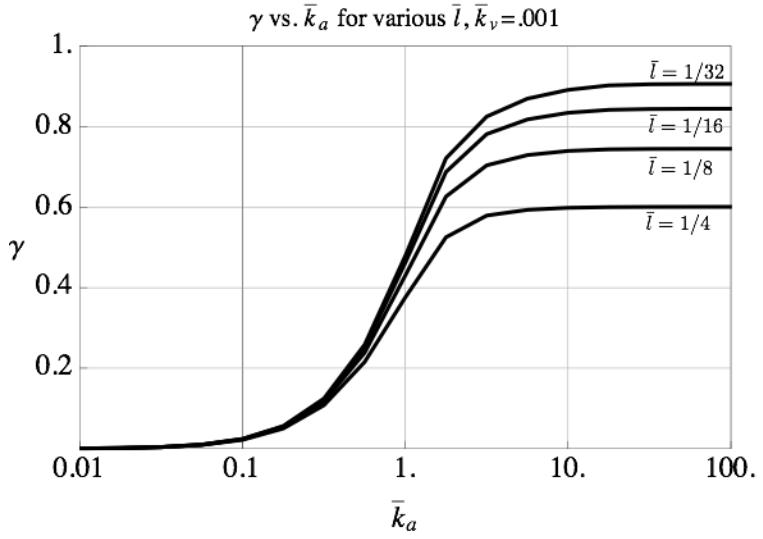

Figure 3. γ vs. $\bar{k}_a$. The coupling parameter, γ, is plotted against the normalized magnetosonic wavenumber, $\bar{k}_a$, for various normalized stand-off lengths, $\bar{l}$. Coupling (and therefore the total thrust coefficient), decrease for smaller wavenumbers. Coupling improves for larger wavenumbers and reaches a maximum dependent on the stand-off length, $\bar{l}$.

The scaling behavior of γ, and thus the thrust coefficient, with respect $\bar{k}_a$ is shown in Figure 3. For varying stand-off lengths, we see that coupling is always maximized for $\bar{k}_a \gg 1$ and that $\gamma \to 0$ as $\bar{k}_a$ becomes small. That is, the best coupling occurs when the wavelength of the targeted mode is smaller than the size of the thruster. However, we have shown previously that values of γ as low as 1/20 can still result in efficient operation for moderate power levels below 5 kW.[1] As result, even as we leave the ray optic regime, reasonable values of γ can be achieved.

V. Magnetosonic Wave Propagation and Absorption

While the magnetosonic wave is well-suited for transferring momentum to a plasma, an effective accelerator must couple this momentum into the bulk particles to create high exhaust velocity. However, major collisionless absorption mechanisms for the magnetosonic wave occur in high beta plasmas,[14] whereas our device is designed to operated with $p_B \gg p_{th}$, i.e., $\beta \ll 1$. This necessitates an understanding of how the wave propagates into the exit region of the thruster to ensure that wave momentum is not reflected and can be transferred into the exhaust.

Since the regime of best coupling corresponds to small wavelengths, we will restrict our analysis to 1D ray optics of the cold magnetosonic wave initially well below the lower hybrid frequency, where the dispersion relation is given by Equation 14. We can then determine the plume structure by calculating the steady state energy and mass fluxes, which must remain constant. A previous attempt to examine waves-based thrusters through the ponderomotive force[2] ignored this mass continuity, which must be taken into account to generate an accurate description of the wave propagation.

The energy flux of the wave is

$$\dot{\mathcal{E}} = v_g \mathcal{E} = v_A \mathcal{E}, \tag{37}$$

where the energy density is

$$\mathcal{E} = \frac{|\tilde{B}|^2}{2\mu_0}. \tag{38}$$

The mass flux driven by the wave is

$$\dot{\mathcal{M}} = \langle \tilde{\rho}\tilde{v} \rangle, \tag{39}$$

which neglects any wall losses and assumes the wave dynamics dominate the system. Time-averaging and combining with Equation 11, we find

$$\dot{\mathcal{M}} = \frac{1}{2}\rho_0 v_A \frac{|\tilde{B}|^2}{\bar{B}^2} = \frac{1}{v_A}\frac{|\tilde{B}|^2}{2\mu_0}. \tag{40}$$

Because $\dot{\mathcal{E}}$ and $\dot{\mathcal{M}}$ are constant throughout the channel, $\tilde{B}$ and v_A must remain constant as well. Thus, if the background magnetic field is also constant throughout the channel, the background density remains uniform, which is simply the case of a plane wave propagating through a uniform medium.

However, as the background magnetic field decays into the exhaust region, the plasma density must decay as well to preserve a constant v_A. In effect, when the plume dynamics are governed primarily by the propagating wave, the plasma configuration maintains a constant impedance. This tendency is particularly beneficial, as it allows the wave momentum and energy to propagate into the plume without adverse reflections on the confining magnetic field structure that might prevent momentum transfer into the exhaust. Additionally, since plasma flows across field lines primarily when $c \gg v_A$,[15] it is beneficial that the Alfvén velocity does not increase in the plume.

From the linearized equations, we can also calculate the perturbed plasma velocity and density:

$$\tilde{v} = v_A \frac{|\tilde{B}|}{\bar{B}} \tag{41}$$

$$\tilde{\rho}/\bar{\rho} = \frac{|\tilde{B}|}{\bar{B}}. \tag{42}$$

As the background field decays, $\tilde{v}$ and $\tilde{\rho}/\bar{\rho}$ both increase, and the wave eventually becomes nonlinear when $\bar{B}$ approaches $\tilde{B}$. However, the channel can be constructed such that this occurs far from the wave-launching antenna, preventing adverse effects on antenna-plasma coupling. As the non-linear regime is reached, the plasma oscillations consist of high density regions with velocities near v_A and low density rarefactions with corresponding negative velocities. This scenario is qualitatively similar to a magnetic beach.[11]

As the wave propagates into the region with lower background $\bar{B}$, it can also reach the lower hybrid resonance where it will be absorbed by the bulk of the plasma. This can be seen in Figure 4, in which we plot the index of refraction for a magnetosonic wave at a given frequency as a function of the background magnetic field at a fixed Alfvén velocity. Initially, at higher magnetic fields in the channel, the index of refraction - and thus the phase velocity - remains constant. As the background magnetic field decays, the lower hybrid frequency shifts towards the excitation frequency, and the index of refraction increases rapidly towards the resonance condition.

VI. Peclet Number for Confinement and Acceleration

In the previous section, we assumed that the wave dynamics were the dominant effect responsible for mass flow in the system. This can be achieved when wave-driven mass advection is large compared to wall losses inside the thruster channel. An anisotropic Péclet number relating these quantities can be defined as

$$Pec = \frac{v_{\text{eff}}/L}{D_\perp/W^2}, \tag{43}$$

where $D_\perp$ is the cross-field diffusion coefficient, v_{eff} is the effective velocity associated with wave-driven mass flow, and L and W are the channel length and height respectively. Effectively, the Péclet number is a ratio of the typical time it takes for a particle to reach the walls compared to the time it takes to be pushed by the wave processes out of the thruster. Thus, for waves to dominate the channel dynamics,

$$Pec \gg 1. \tag{44}$$

The cross-field diffusion coefficient can be calculated classically[16–18] such that

$$D_\perp = \frac{p_e}{\sigma_e B_0^2}, \tag{45}$$

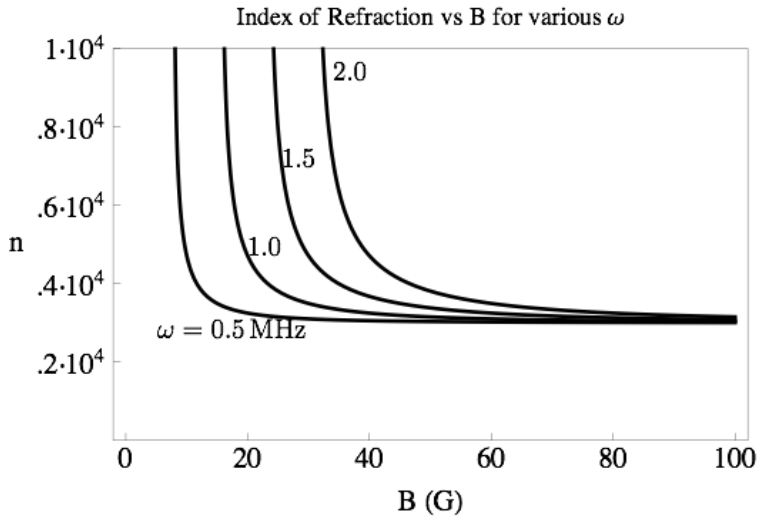

Figure 4. Index of Refraction vs. Magnetic Field for the cold magnetosonic wave. The density is assumed to vary with the magnetic field so that $v_A = 10^5\,\mathrm{m/s}$ remains constant. Away from resonance, $n = 3000$. For high frequencies, as B is decreased, the lower hybrid resonance is reached sooner.

where $\sigma_e = \frac{e^2 n_e}{m_e \nu_e}$. The effective velocity can be calculated by the total particle flux associated with the propagating wave-mode divided by the background density, i.e.,

$$v_{\text{eff}} = \dot{\mathcal{M}}_{\text{wave}}/\rho_0. \tag{46}$$

From the linearized continuity equation and Equation 39, we find

$$\dot{\mathcal{M}}_{\text{wave}} = \frac{1}{2} v_A \frac{\tilde{\rho}^2}{\rho_0}. \tag{47}$$

Therefore,

$$v_{\text{eff}} = \frac{1}{2} v_A \frac{\tilde{\rho}^2}{\rho_0^2} = \frac{1}{2} v_A \frac{\tilde{B}^2}{B_0^2}. \tag{48}$$

Combining Equations 43, 45, and 48, we get

$$Pec = \frac{1}{2} \frac{W^2}{L} v_A \frac{\sigma_e \tilde{B}^2}{p_e}. \tag{49}$$

Qualitatively, there is a minimum wave amplitude, $\tilde{B}$, for which Equation 44 is satisfied, and the channel flow becomes wave dominated. This can be related directly to the total power required by noting that wave energy flux is

$$\dot{\mathcal{E}} = v_A \mathcal{E} = v_A \frac{\tilde{B}^2}{2\mu_0}, \tag{50}$$

and the total wave power is

$$P = WH\dot{\mathcal{E}} = WH v_A \frac{\tilde{B}^2}{2\mu_0}. \tag{51}$$

To satisfy Equation 44, the wave power must be greater than a critical value. That is, $P \gg P^*$, where

$$P^* = \frac{LH}{W} \frac{p_e}{\mu_0 \sigma_e} = \frac{LH}{W} \frac{T_e m_e \nu_e}{\mu_0 e^2}. \tag{52}$$

For a 10 cm thruster with $T_e = 5\,\mathrm{eV}$ and $n_e = 10^{18}\,\mathrm{m}^{-3}$, this corresponds to a critical power level of only 6 W.

VII. DWDT Design Considerations

In this paper, we have analyzed a magnetosonic mode driven DWDT to determine the relevant critical parameters for effective operation. First, we have shown that the the antenna-plasma coupling is strongly dependent on, $\bar{k}_a$, the ratio of the magnetosonic wavelength to the size of the thruster. The coupling is uniform and maximized in the limit of the ray optic regime where $\bar{k}_a \gg 1$. However, efficient thruster operation can still theoretically be achieved for $\bar{k}_a \sim 1$.

Because the acceleration mechanism is naturally directed across magnetic field lines, it is important that we ensure the that flow successfully detaches from the applied field. In their ponderomotive DWDT concept, Jorns and Choueiri proposed that charge separation in the channel could allow for the momentum to be transferred across magnetic field lines.[2] This has been shown previously by Peter and Rostoker[15] to be possible, as long as the $\epsilon_\perp \gg 1$, which corresponds to $v_A \ll c$. The magnetosonic mode driven DWDT operates at exhaust velocities appropriate for propulsive applications only when this criterion is satisfied. Moreover, since the Alfvén velocity remains constant in a wave-dominated thruster, this criterion remains satisfied into the exhaust plume.

Finally, we have shown an appropriate condition for a wave-dominated thruster can be described by an anisotropic Péclet number which compares the wave-advected mass flux to the diffusion losses to the walls. Pec depends primarily on the electron temperature and collision frequency, and is therefore not a parameter we can strongly control. However, for reasonable expected plasma parameters of an electric propulsion device, the total power required to reach a wave-dominated condition is easily achievable.

This paper laid out the framework for analyzing a general DWDT. The analysis performed for the magnetosonic wave was deliberately simplified to elucidate key criteria for thruster performance. The immediate goal is to validate these models and scaling behaviors with a proof-of-concept experiment. From there, future efforts can focus on fully kinetic descriptions of the plasma response, in order to improve the model further.

Appendix A

We will present the derivation of the solution to the normalized vector potential. Starting from Equation 21,

$$\bar{\nabla}^2 \bar{A}_y + \bar{K}^2 \bar{A}_y = 0, \tag{53}$$

and applying separation of variables, such that $\bar{A}_y(\bar{x}, \bar{z}) = X(\bar{x}) \cdot Z(\bar{z})$, we have

$$X''(\bar{x}) = (-\bar{K}^2 + a^2)X, \tag{54}$$

$$Z''(\bar{z}) = -a^2 Z, \tag{55}$$

where a is a separation constant which must be integrated over to form a complete solution. From the symmetry of the geometry given,

$$Z \sim \cos(a\bar{z}), \tag{56}$$

$$X \sim e^{\pm i\sqrt{K^2 - a^2}\bar{x}}, \tag{57}$$

where X can take on either mode in region 2, but can only represent outward propagating modes in regions 1 and 3. That is, no energy is coming into the system from infinity. Therefore, the piecewise solution of $\bar{A}_y$ is generated by integrating over all possible separation constants and takes the form given in Equations 23-25,

$$\bar{A}_{y1}(\bar{x}, \bar{z}, \bar{k}_v, \bar{k}_a, \bar{l}) = \int_0^\infty C_1 e^{-i\bar{k}_1\bar{x}} \cos(a\bar{z}) da, \tag{58}$$

$$\bar{A}_{y2}(\bar{x}, \bar{z}, \bar{k}_v, \bar{k}_a, \bar{l}) = \int_0^\infty (C_2 e^{i\bar{k}_1\bar{x}} + C_3 e^{-i\bar{k}_1\bar{x}}) \cos(a\bar{z}) da, \tag{59}$$

$$\bar{A}_{y3}(\bar{x}, \bar{z}, \bar{k}_v, \bar{k}_a, \bar{l}) = \int_0^\infty C_4 e^{i\bar{k}_2\bar{x}} \cos(a\bar{z}) da. \tag{60}$$

A solution is found by matching boundary conditions between each region. At each interface, $\bar{A}_y$ and its derivative must be continuous, except for a jump discontinuity across the wave-launching antenna. To form the full antenna, we start with a pair of wires at heights, $\bar{z} = \pm\bar{h}$. After finding the individual solution, we then integrate over a continuous current density in an antenna of size H. For wires at $\bar{z} = \pm\bar{h}$, the boundary conditions are:

$$\int_0^\infty D_1 \cos(a\bar{z})da = \int_0^\infty D_2 \cos(a\bar{z})da + \int_0^\infty D_3 \cos(a\bar{z})da, \tag{61}$$

$$\int_0^\infty -i\bar{k}_1 D_1 \cos(a\bar{z})da = \int_0^\infty i\bar{k}_1 D_2 \cos(a\bar{z})da + \int_0^\infty -i\bar{k}_1 D_3 \cos(a\bar{z})da - \delta(\bar{z}-\bar{h}) - \delta(\bar{z}+\bar{h}), \tag{62}$$

$$\int_0^\infty D_2 \cos(a\bar{z})e^{i\bar{k}_1\bar{l}}da + \int_0^\infty D_3 \cos(a\bar{z})e^{-i\bar{k}_1\bar{l}}da = \int_0^\infty D_4 \cos(a\bar{z})e^{i\bar{k}_2\bar{l}}da, \tag{63}$$

$$\int_0^\infty i\bar{k}_1 D_2 \cos(a\bar{z})e^{i\bar{k}_1\bar{l}}da + \int_0^\infty -i\bar{k}_1 D_3 \cos(a\bar{z})e^{-i\bar{k}_1\bar{l}}da = \int_0^\infty i\bar{k}_2 D_4 \cos(a\bar{z})e^{i\bar{k}_2\bar{l}}da, \tag{64}$$

where D_i represents the constants associated with a wire pair and C_i represents the constants associated with the full antenna.

Noting that $\int_0^\infty \cos(a\bar{z})da = \pi\delta(\bar{z})$, we can solve this system to find that:

$$D_1 = \frac{1}{i\pi}\cos(a\bar{h})\frac{1}{\bar{k}_1}\left(1 + \frac{\bar{k}_1 - \bar{k}_2}{\bar{k}_1 + \bar{k}_2}e^{2i\bar{k}_1\bar{l}}\right), \tag{65}$$

$$D_2 = \frac{1}{i\pi}\cos(a\bar{h})\frac{1}{\bar{k}_1} \tag{66}$$

$$D_3 = \frac{1}{i\pi}\cos(a\bar{h})\frac{e^{2i\bar{k}_1\bar{l}}}{\bar{k}_1}\frac{\bar{k}_1 - \bar{k}_2}{\bar{k}_1 + \bar{k}_2}, \tag{67}$$

$$D_4 = \frac{2}{i\pi}\cos(a\bar{h})\frac{e^{i(\bar{k}_1 - \bar{k}_2)\bar{l}}}{\bar{k}_1 + \bar{k}_2}. \tag{68}$$

The C_i coefficients can then be found by integrating the current density over an infinite stack of wire pairs for h between 0 and H (or 0 and 1 in the normalized $\bar{h}$ coordinate). Using

$$C_i = \int_0^1 D_i d\bar{h}, \tag{69}$$

we obtain the results given in Equations 28-31, i.e.,

$$C_1 = \frac{1}{i\pi}\frac{\sin a}{a}\frac{1}{\bar{k}_1}\left(1 + \frac{\bar{k}_1 - \bar{k}_2}{\bar{k}_1 + \bar{k}_2}e^{2i\bar{k}_1\bar{l}}\right), \tag{70}$$

$$C_2 = \frac{1}{i\pi}\frac{\sin a}{a}\frac{1}{\bar{k}_1} \tag{71}$$

$$C_3 = \frac{1}{i\pi}\frac{\sin a}{a}\frac{e^{2i\bar{k}_1\bar{l}}}{\bar{k}_1}\frac{\bar{k}_1 - \bar{k}_2}{\bar{k}_1 + \bar{k}_2}, \tag{72}$$

$$C_4 = \frac{2}{i\pi}\frac{\sin a}{a}\frac{e^{i(\bar{k}_1 - \bar{k}_2)\bar{l}}}{\bar{k}_1 + \bar{k}_2}. \tag{73}$$

Acknowledgments

This research was supported by a Strategic University Partnership Research (SURP) grant provided by the Jet Propulsion Laboratory, California Institute of Technology, under a contract with the National Aeronautics and Space Administration, as well as the Program in Plasma Science and Technology (PPST) at Princeton University.

References

[1]Feldman, M.S., Choueiri, E.Y. "The Direct Wave-Drive Thruster," 50^{th} Joint Propulsion Conference, Cleveland, OH, Number AIAA-2014-4025, July 28-30, 2014.

[2]Jorns, B. and Choueiri, E.Y., "Thruster concept for transverse acceleration by the beating electrostatic waves ponderomotive force," 32^{nd} International Electric Propulsion Conference, Number IEPC-2011-214, September 11-15, 2011.

[3]Stallard, B.W., Hooper, E.B., Power, J.L., "Whistler-driven, electron-cyclotron-resonance-heated thruster - Experimental status," *Journal of Propulsion and Power*, Volume 12, No. 4, 1996.

[4]Diaz, F.R.C., "The Vasimr Rocket," *Scientific American*, Volume 283, pp90-97, November 2000.

[5]Pavarin, D., Ferri, F., et. al., "Design of a 50W Helicon Plasma Thruster," 31^{st} International Electric Propulsion Conference, Number IEPC-2009-205. September 20 - 24, 2009.

[6]Lovberg, R. H., Dailey, C. L., "PIT Mark V Design." Number AIAA 1991-3571, September 1991.

[7]Choueiri, E., Polzin, K., "Faraday Accelerator with Radio-frequency Assisted Discharge (FARAD)." Number AIAA 2004-3940, July 2004.

[8]Motz, H., Watson, C.J.H., *Advances in Electronics and Electron Physics*, Volume 23, Academic Press, "The Radio-frequency Confinement of Plasmas," p264-282, 1967.

[9]Jorns, B. and Choueiri, E.Y., "A Plasma Propulsion Concept Based on Direct Ion Acceleration with Beating Electrostatic Waves," 46^{th} Jnt. Prop. Conf. Number AIAA-2010-7107, July 2010.

[10]Dodin, I.Y., and Fisch, N.J., "Axiomatic Geometrical Optics, Abraham-Minkowski controversy and photon properties derived classically," *Phys. Rev. A*, Vol 86 Issue 5, Number 053834. November 2012.

[11]Stix, T.H., *Waves in Plasmas* AIP Press, p342-343, 1992.

[12]Dodd, C.V., Deeds, W.E., "Analytical Solutions to the EddyCurrent ProbeCoil Problems," *Journal of Applied Physics*, Volume 39, 1968.

[13]Skiff, F., Ono, M., Wong, K.L., "Excitation of ion Bernstein waves from loop antennas," *Physics of Fluids* Volume 31, 2030, 1988.

[14]Barnes, A., "Collisionless Damping of Hydromagnetic Waves," *Physics of Fluids*, Volume 9, 8, 1966.

[15]Peter, W., Roster, N., "Theory of plasma injection into a magnetic field," *Physics of Fluids* Volume 25, 730, 1982.

[16]Chen, F.F., *Introduction to Plasma Physics and Controlled Fusion*, 2nd ed., Springer 1984.

[17]Little, J.M., "Critical Condition for Plasma Confinement in the Source of a Magnetic Nozzle Flow," *IEEE Transactions on Plasma Science*, Volume 43, 1, Jan. 2015, p277-286.

[18]Chen, F.F., "Experiments on helicon plasma sources," *Journal of Vacuum Science Technology A*, Volume 10, 4, 1992.